

**inter-noise 2008**

*From Silence to Harmony*

**37th International Congress and Exposition on Noise Control Engineering  
26-29 October 2008·Shanghai·China**

## **CHARACTERIZATION OF THE AUDIBLE MAGNETIC NOISE EMITTED BY TRACTION MOTORS IN RAILWAY ROLLING STOCK**

J. Le Besnerais<sup>a,b</sup>, V. Lanfranchi<sup>c</sup>, M. Hecquet<sup>b</sup>, S. Récorbet<sup>a</sup>, J.  
Sapena<sup>a</sup>, P. Brochet<sup>b</sup>

<sup>a</sup> ALSTOM Transport, 50 r doct Guinier, 65600 SEMEAC, France

<sup>b</sup> Laboratoire d'Electrotechnique et d'Electronique de Puissance de Lille (L2EP),  
Ecole Centrale de Lille, Cité Scientifique, Villeneuve d'Ascq, France

<sup>c</sup> Laboratoire d'Electromécanique de Compiègne (LEC), Université de  
Technologie de Compiègne, Compiègne, France

### **ABSTRACT**

This paper first presents the analytical models of an ALSTOM simulation software, DIVA, which computes the vibratory and acoustic behavior of a variable-speed induction machine due to Maxwell forces. This radial magnetic pressure in the air-gap makes the stator vibrate in the audible range, creating the so-called magnetic noise characterized by a high tonality.

On the ground on these analytical models, the main magnetic vibrations due to slotting, pulse-width modulation (PWM) harmonics and their interaction are then analytically characterized. Their number of nodes, velocity and propagation direction are experimentally validated by visualizing the stator deflection shapes.

Finally, some experimental validations of the simulation tool are presented. On the ground of both analytical results and simulations, it is shown that some quieter motors can be designed acting on the motor geometry (especially slot numbers) and PWM strategy.

### **1 INTRODUCTION**

Sustainable mobility requires environment-friendly and human-friendly electrical transport systems. As a consequence, acoustic comfort is an increasingly important factor at the design stage of ALSTOM traction motors. Their acoustic noise can come from aerodynamic noise (fans, windage noise, ...), mechanical noise (bearings, ...) and magnetic noise which is caused by magnetic forces acting on the active materials of the machine. In some cases, the global sound power level (SPL) is controlled by the magnetic noise radiated by the motor. This noise can be quickly annoying as its spectrum contains high tonalities: some frontage residents complaints have been already recorded in a light rail vehicle application and these tonalities are restricted in the last years by operators requirements.

Indeed, once the motor aerodynamic noise has been reduced, the acoustic noise of magnetic origin dominates more frequently the SPL. Moreover, passengers tend to be placed closer to the motor in order to higher the transport capacity, they are therefore more exposed to magnetic noise. In starting phase, the aerodynamic source of noise is also very low as the fan rotates at the motor speed, which makes the magnetic noise more perceivable. Finally, the successive PWM strategies employed during starting significantly enrich the magnetic noise

---

<sup>a</sup> Email address: jean.le\_besnerais@centraliens.net

<sup>b</sup> Email address: michel.hecquet@ec-lille.fr

<sup>c</sup> Email address: vincent.lanfranchi@utc.fr

spectrum with high frequency harmonics (1 kHz to 6 kHz). Understanding the magnetic noise generation process when associating a traction motor to an inverter, and establishing some low-noise design rules is then crucial to meet the operators requirements in terms of acoustic comfort for both passengers (including the driver) and frontage residents.

To help ALSTOM engineers integrating the noise factor at the design stage of traction motors, and to diagnose magnetic noise problems occurring on running motors, a simulation tool called DIVA has been developed. It is able to compute the audible magnetic noise sound power level radiated by a motor in function of its speed, PWM strategy and geometry. In a first part, this paper will therefore detail the electromagnetic, mechanical and acoustic models used in the software DIVA.

On the ground of these analytical models are then characterized all the magnetic vibration waves in terms of frequency (including the propagation direction), and number of nodes (or spatial order). This is especially important as resonance occurs when a force line of spatial order  $m$  and frequency  $f$  meets the stator sheets circumferential mode  $m$  of natural frequency  $f$ . Among these vibrations will be distinguished vibrations due to slotting, PWM harmonics, and their interaction. These analytical expressions are validated experimentally by visualizing the stator deflection shapes.

Finally, an experimental validation of the simulation tool is showed by comparing the measured and simulated sonagrams, and some example of low-noise motor design guidelines are presented. Two ALSTOM prototypes have been built, and experimental results will be detailed in a future contribution.

## 2 ANALYTICAL MODELS OF THE SIMULATION TOOL

Among magnetic forces, magnetostrictive forces and Laplace forces are neglected, and stator vibrations are assumed to be caused by the Maxwell force radial component, which can be approximated proportionally to the square flux density. The electromagnetic part of DIVA therefore aims at determining the radial flux density distribution.

### 2.1 Electromagnetic model

The air-gap radial flux density  $B_g$  computation is decomposed as [6]

$$B_g(t, \alpha_s) = \Lambda(t, \alpha_s)(f_{mm}^s(t, \alpha_s) + f_{mm}^r(t, \alpha_s)) \quad (1)$$

$\Lambda$  is the permeance per unit area, given by

$$\Lambda(t, \alpha_s) = \frac{\mu_0}{g_f(t, \alpha_s)} \quad (2)$$

where  $\mu_0$  is the air magnetic permeability, and  $g_f$  is the mean flux density line length, approximated as a piecewise constant function which takes four different values ( $g$ ,  $g+p_s$ ,  $g+p_r$ ,  $g+p_r+p_s$ ) according to the rotor and stator slot relative position [4]. The permeance is modified in saturated case to account for the flattening of the air-gap flux density [22], which modifies the magnetic forces spectrum. Saturation phenomenon can actually strongly influence the magnetic noise level.

$f_{mm}^s$  and  $f_{mm}^r$  are the stator and rotor magnetomotive forces (mmf) computed as

$$f_{mm}^s(t, \alpha_s) = \sum_{q=1}^{q_s} i_q^s(t) N_q^s(\alpha_s) \quad f_{mm}^r(t, \alpha_s) = \sum_{b=1}^{Z_r} i_b^r(t) N_b^r(t, \alpha_s) \quad (3)$$

where  $i_q^s$  and  $i_b^r$  are the stator  $q$ -th phase and rotor  $b$ -th bar currents, and  $N_q^s$  and  $N_b^r$  are the stator and rotor winding functions [3],  $Z_r$  being the number of rotor bars, and  $q_s$  being the number of stator phases.

Stator and rotor currents are computed from the knowledge of the PWM supply phase voltage, using an equivalent electrical circuit of the motor extended to time harmonics [9] (see Figure 1). A global saturation coefficient is computed to account for the magnetization inductance decrease with saturation [20].

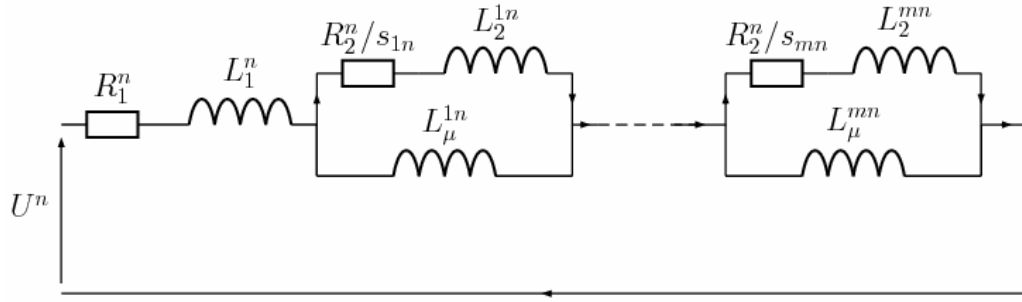


Figure 1: Single phase equivalent circuit of the  $n$ -th time harmonic layer.  $U^n$  is the  $n$ -th component of the supply phase voltage spectrum at frequency  $f_n$ , and  $s_{mn}=1-mf_0(1-s)/f_n$  stands for the harmonic slip of the  $m$ -th space harmonic and  $n$ -th time harmonic,  $s$  being the fundamental slip.

Examples of stator winding functions, stator mmf, rotor mmf, permeance and air-gap flux density distributions in sinusoidal case are shown in Figure 2 to 4 for a motor with  $Z_s=36$  stator slots,  $Z_r=28$  rotor slots, and  $p=3$  pole pairs.

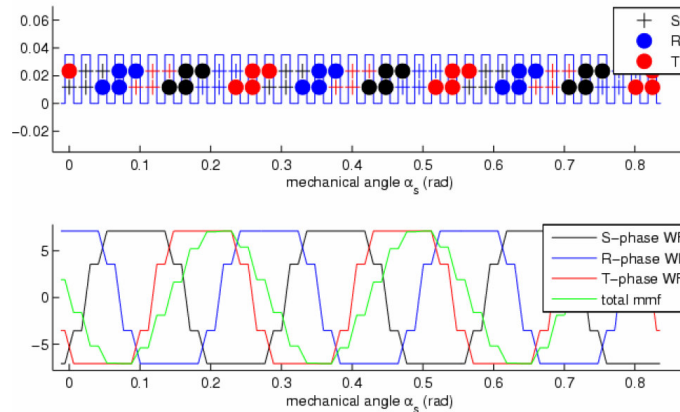


Figure 2: Stator winding pattern (shorted pitch 5/6), associated winding function (WF) and total mmf distributions along the air-gap.

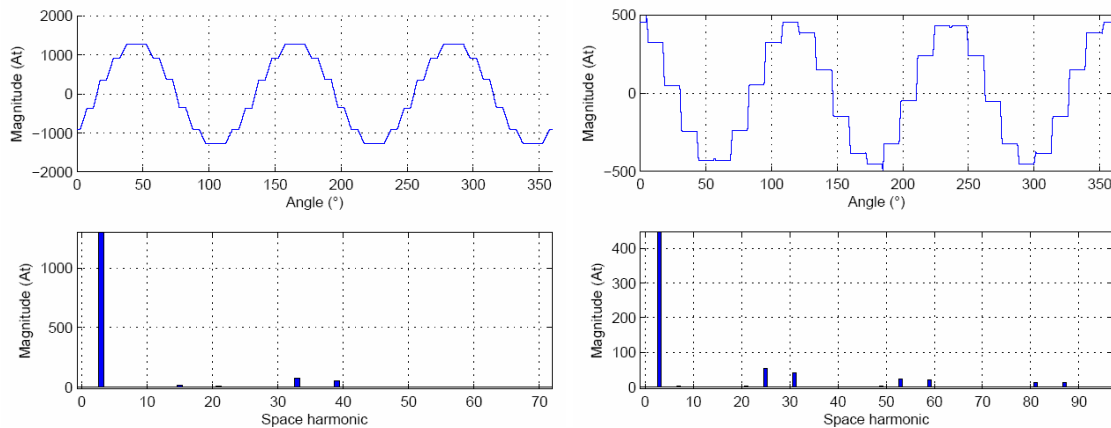


Figure 3: Stator (left) and rotor (right) mmf distributions along the air-gap, and their space harmonic contents.

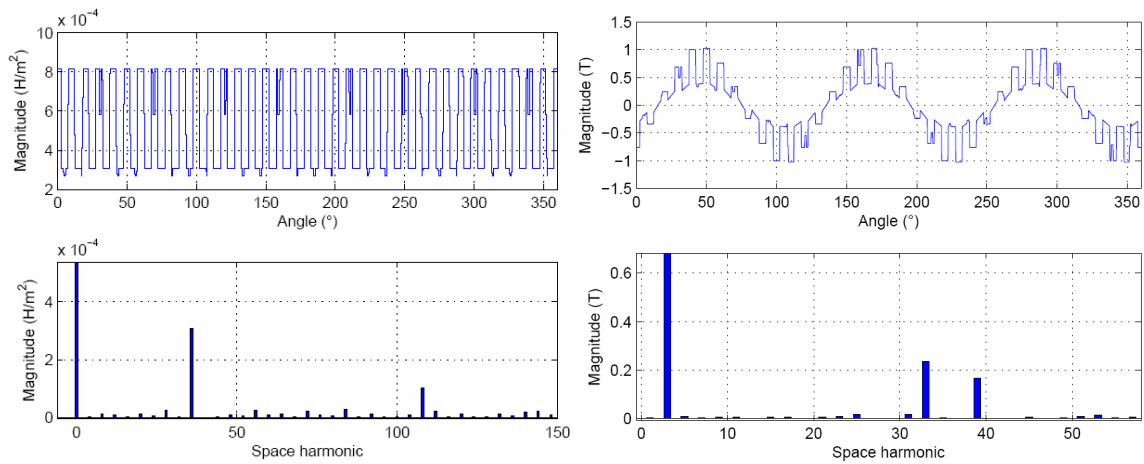


Figure 4: Permeance (left) and flux-density (right) distributions along the air-gap, and their space harmonic contents.

The resulting Maxwell pressure is expressed as

$$P_M = B_g(t, \alpha_s)^2 / (2\mu_0) \quad (4)$$

Its distribution along the air-gap is illustrated in Figure 5: we can see that it tends to pull stator teeth towards the rotor.

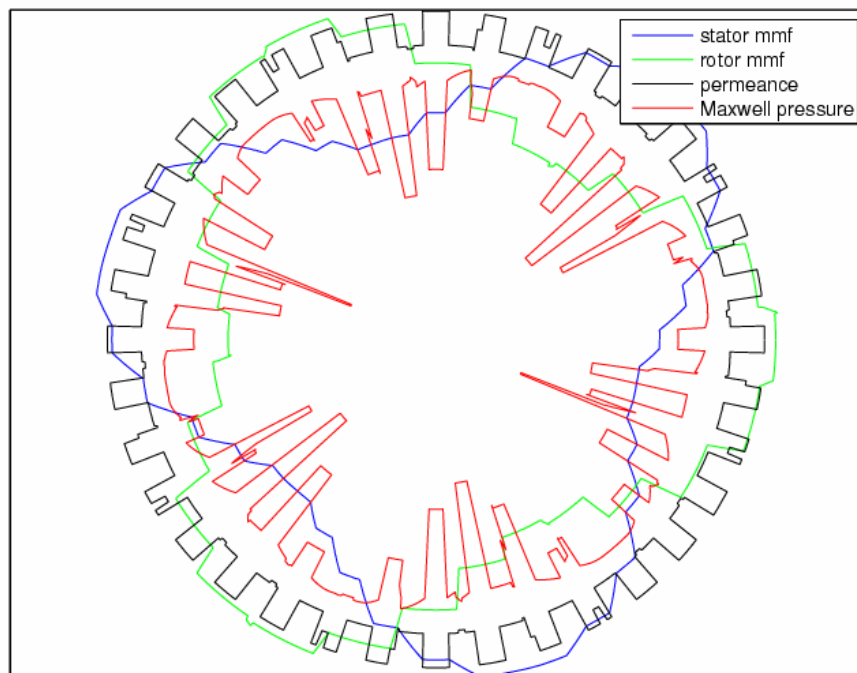


Figure 5: Stator and rotor mmf, permeance and resulting Maxwell pressure distributions along the air-gap.

Currents computation, in on-load, saturated or PWM cases have been validated with tests. The flux density distribution was validated using finite element method (FEM) software FLUX2D [15,16].

## 2.2 Mechanical model

The force distribution is developed into a 2D Fourier series of force waves  $P_{mw}$  with spatial frequencies (spatial order)  $m$  and frequency  $f$  (Figure 6).

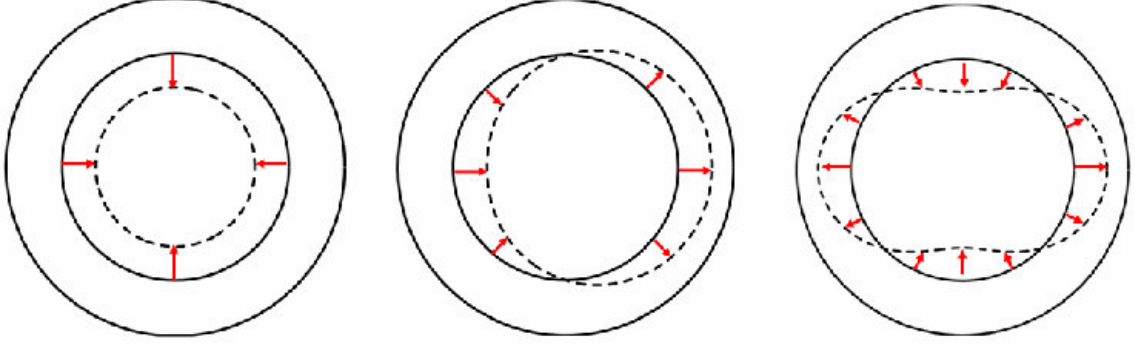


Figure 6: Illustration of the pressure distribution decomposition in sinusoidal force waves of order 0, 1 and 2.

The stator is then modeled as a 2D ring, and its static deflections under the sinusoidal loads  $P_{mw}$  can be analytically computed. For instance, for  $m > 1$

$$Y_{mw}^s = 12R_a R_m^3 P_{mw} / (Eh^3 (m^2 - 1)^2) \quad (5)$$

where  $h$  is the thickness of the stator back core (yoke),  $R_m$  is the mean stator radius (computed without considering the teeth),  $E$  is the stator's Young modulus in radial direction and  $R_a$  is the stator bore radius. Then, dynamic displacements  $Y_{mw}^d$  are computed through a second order transfer function:

$$Y_{mw}^d = Y_{mw}^s \left[ (1 - f^2 / f_m^2)^2 + 4\zeta_m^2 f^2 / f_m^2 \right]^{-1/2} \quad (6)$$

where  $\zeta_m$  is the damping coefficient, and  $f_m$  is the  $m$ -th stator circumferential mode natural frequency.  $\zeta_m$  lie between 1% and 4%, it is computed using the experimental established by Yang [27]. The natural frequencies are computed modeling the stator sheet as a 2D ring. For  $m \geq 2$  they are expressed as [7]:

$$f_m = f_0 h m (m^2 - 1) / (2\sqrt{3} R_m \sqrt{m^2 + 1}) \quad f_0 = \sqrt{E / (\Delta \rho)} / (2\pi R_m) \quad (7)$$

where  $f_0$  is the zero mode natural frequency,  $\rho$  is the stator mass per unit volume, and  $\Delta$  is the stator mass corrective factor which includes the effect of windings and teeth mass.

The natural frequencies computation was validated by FEM and tests [9,14,17], with some operational or experimental modal analysis.

### 2.3 Acoustic model

The velocity vibration waves  $v_{mw}$  are then computed as

$$v_{mw} = \omega Y_{mw}^d \quad (8)$$

and the associated radiated power is

$$W_m(f) = \rho_0 c S \sigma_m(f) |v_{mw}|^2 / 2 \quad (9)$$

where  $\sigma_m$  is the radiation factor,  $\rho_0$  the air density,  $c$  the speed of sound and  $S$  the stator outer

surface including frame. The radiation factor computation is analytically computed using the model of a pulsating sphere [25]. The total sound power  $W(f)$  is the sum of the sound power radiated by each mode. The total sound power level associated to a given frequency is then

$$L_w(f) = 10 \log_{10}(W(f)/W_0), \quad W_0 = 10^{-12} W \quad (10)$$

and the global A-weighted sound power level, accounting for the variation of human's ear sensitivity with frequency, is obtained as

$$L_{wA} = 10 \log \left( \sum_f 10^{0.1w_A(f)L_w(f)} \right) \quad (11)$$

where  $w_A(f)$  stands for the A-weight at frequency  $f$ .

Note that the ALSTOM software DIVA is very fast (a few seconds on a 2GHz laptop). More details about the models and their implementation can be found in [14].

### 3 MAGNETIC NOISE CHARACTERISATION

Equation (5) shows that the stator deflections quickly decrease with the mode number. As a consequence, the strongest magnetic vibrations occurring on traction motors are of order 0, 2 or 4. It therefore important to be able to predict which force waves have 0, 2, or 4 orders, at which frequencies they occur and whether they will resonate or not with the stator modes during starting phase.

To achieve this goal, the analytical spectrum of the exciting forces has been fully detailed, including slotting, eccentricities, saturation and PWM effects [14,17,18]. This spectrum is identical to the vibration spectrum, and noise spectrum. This was done by developing in Fourier series the mmf and permeance distributions: each force line is then given by a combination of two flux density waves, i.e. a combination of two permeance harmonics and two mmf harmonics.

#### 3.1 Slotting vibrations

When combining some slotting permeance harmonics with the fundamental stator mmfs, we obtain the so-called slotting harmonics. These slotting forces are null when the rotor and stator slots are closed, and as they are linked to the fundamental current, they remain when supplying the motor with PWM. Their main expression are detailed in Table 1, where  $k_s$  and  $k_r$  are positive integers coming from the Fourier series of permeance distribution (as a consequence, the magnitude of the slotting force is proportional to  $1/(k_r k_s)$  [4]),  $f_s$  is the stator current fundamental frequency, and  $g$  is the fundamental slip. The information of the propagation direction of vibration waves can be introduced with negative frequencies, or negative spatial orders. The latter convention is used in this paper.

Table 1: Main slotting forces characterization.

	Frequency $f$	Spatial order $m$
$F_{s-}$	$f_s(k_r Z_r(1-g)/p-2)$	$k_r Z_r - k_s Z_s - 2p$
$F_s$	$f_s(k_r Z_r(1-g)/p)$	$k_r Z_r - k_s Z_s$
$F_{s+}$	$f_s(k_r Z_r(1-g)/p+2)$	$k_r Z_r - k_s Z_s + 2p$

We can see that the spatial orders of the slotting forces highly depend on the rotor and stator slot combination. The highest magnitude slotting force is given for  $k_s=k_r=1$ : for instance, if

$Z_s=36$ ,  $Z_r=28$  and  $p=3$ , a force line of order  $-2$  ( $=28-36+6$ ) and frequency  $f_s(36(1-g)/p+2)$  occurs. It can therefore potentially resonate with the elliptical mode of the stator.

### 3.2 PWM vibrations

When combining two fundamental permeances with a fundamental stator mmf, and an harmonic mmf due to a PWM time harmonic  $f_n$  of the stator current, we obtain the so-called PWM harmonics. For an intersective asynchronous PWM of switching frequency  $f_c$ , the first group of harmonic currents is  $2f_c \pm f_s$  and the main PWM lines are expressed in Table 2.

Table 2: Main PWM forces characterization (asynchronous case).

	Frequency $f$	Spatial order $m$
$F_{\text{pwm-}}$	$2f_c - 2f_s$	$-2p$
$F_{\text{pwm}}$	$2f_c$	$0$
$F_{\text{pwm+}}$	$2f_c + 2f_s$	$2p$

PWM lines therefore necessarily of orders  $0$  or  $2p$  [21], centered around twice the switching frequency, and independent of the slot numbers. The vibration line  $F_{\text{pwm}}$  is different from the others as it is a standing wave. These lines qualify the PWM noise which is particularly audible at the beginning of the starting phase ( $f_s$  close to  $0$ ).

### 3.3 Slotting PWM vibrations

When combining two permeance slotting harmonics with a fundamental stator mmf, and an harmonic mmf due to a PWM time harmonic  $f_n$  of the stator current, we obtain the so-called slotting PWM harmonics. The main PWM lines are expressed in Table 3 for the asynchronous intersective PWM.

Table 3: Main slotting PWM forces characterization (asynchronous case).

	Frequency $f$	Spatial order $m$
$F_{\text{spwm--}}$	$2f_c \pm f_s(k_r Z_r(1-g)/p-3)$	$k_s Z_s - k_r Z_r + 2p$
$F_{\text{spwm-}}$	$2f_c \pm f_s(k_r Z_r(1-g)/p-1)$	$k_s Z_s - k_r Z_r$
$F_{\text{spwm+}}$	$2f_c \pm f_s(k_r Z_r(1-g)/p+1)$	$k_s Z_s - k_r Z_r$
$F_{\text{spwm++}}$	$2f_c \pm f_s(k_r Z_r(1-g)/p+3)$	$k_s Z_s - k_r Z_r - 2p$

### 3.4 Other vibration lines

Some other important vibration lines can be characterized with the same method, such as winding vibrations, due to mmf space harmonics, saturation vibrations, due to permeance saturation harmonics, and eccentricity vibrations [18].

## 4 VALIDATIONS

### 4.1 Operational Deflection Shapes (ODS)

In order to validate the frequency, number of nodes and propagation direction of all these vibration waves, some the stator operational deflection shapes (ODS) of a stator have been analyzed using Pulse Labshop in the LEC laboratory (Compiègne, France). As an example, Figure 7 shows the deflection shapes associated to the pure PWM lines.

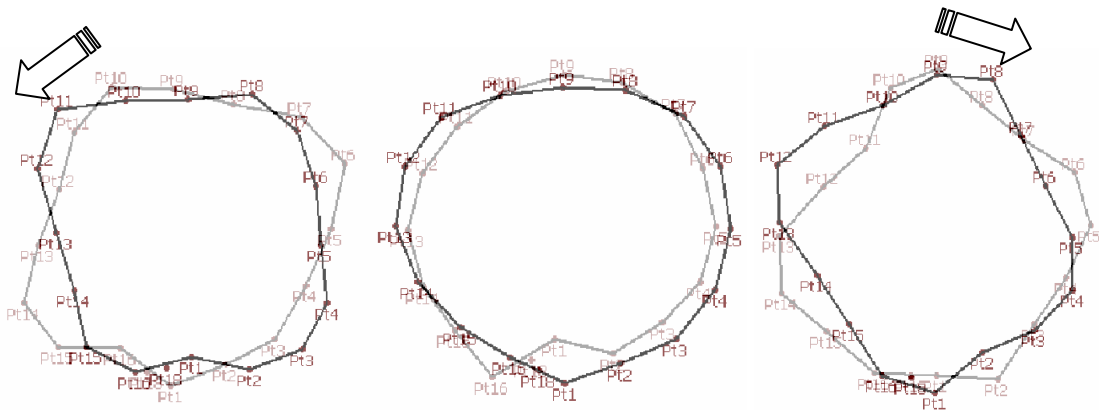


Figure 7: Operational deflection shapes of the stator at the PWM forces frequencies of order  $-2p=4$ ,  $0$  and  $2p=4$ .

#### 4.2 FEM/BEM validation

The vibro-acoustic analytical model has been numerically validated by the company VIBRATEC, partner of the Predit-III ADEME Prosodie project. They coupled a mechanical FEM software (Ideas) to a boundary element method (BEM) software (Sysnoise), and computed the sound power level radiated by the motor equivalent cylinder under some typical magnetic excitations (Figure 8).

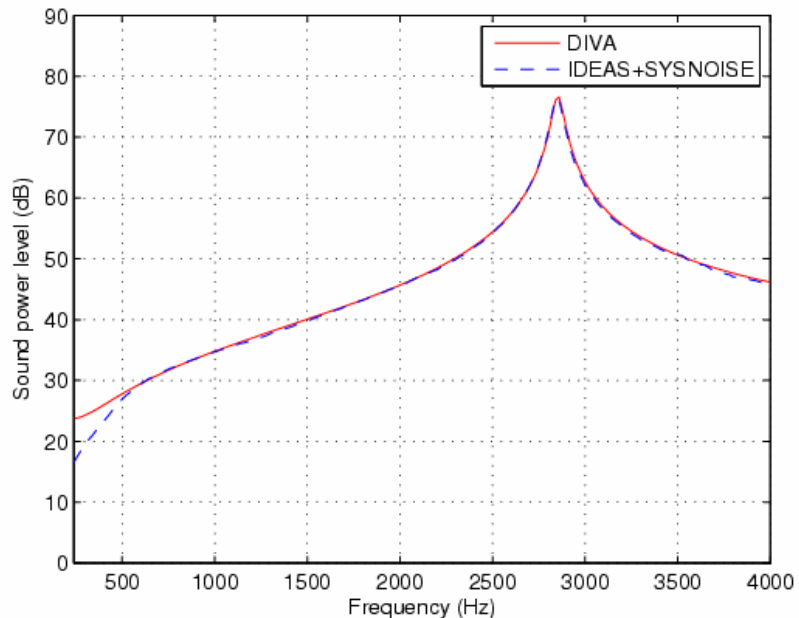


Figure 8: Sound power level computed by DIVA and FEM+BEM (acoustic response to rotating force wave of order 4 with an electrical frequency going from 400 to 4000 Hz).

#### 4.3 Sonagrams

Finally, a simulated sonogram (Figure 10) has been successfully compared to an experimental one (Figure 9) on a 250kW water-cooled traction motor run from 0 to 200 Hz.

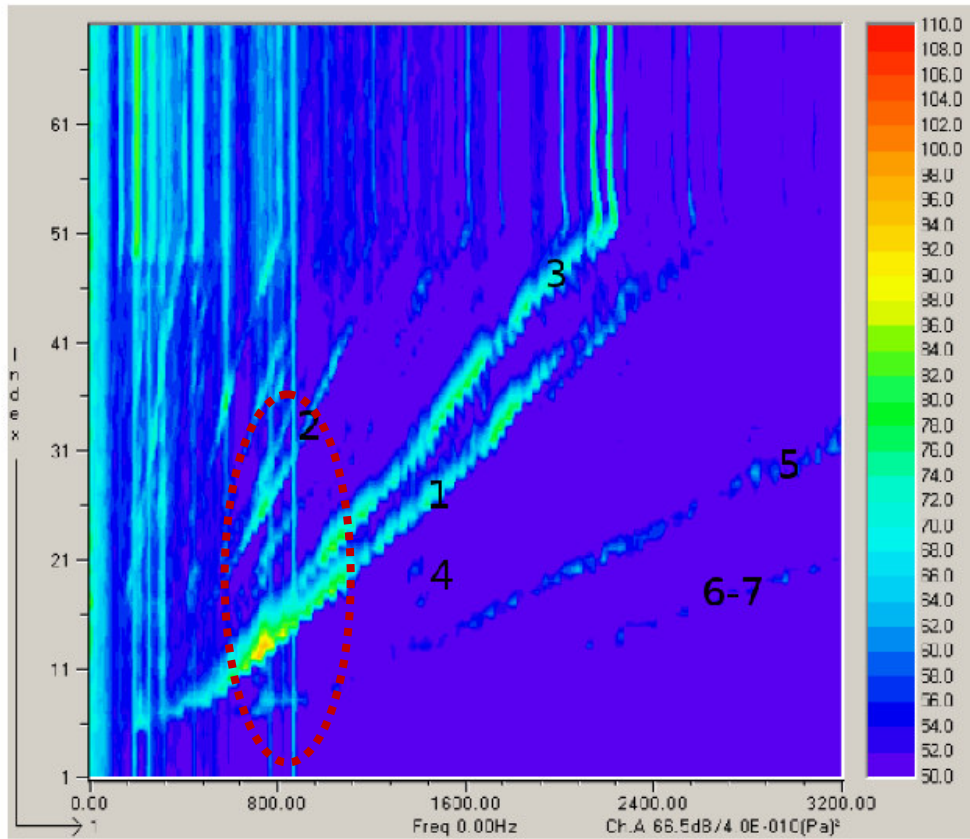


Figure 9: Measured sonogram of a water-cooled 250 kW traction motor in sinusoidal off-load case ( $f_s=0$  to 200 Hz).

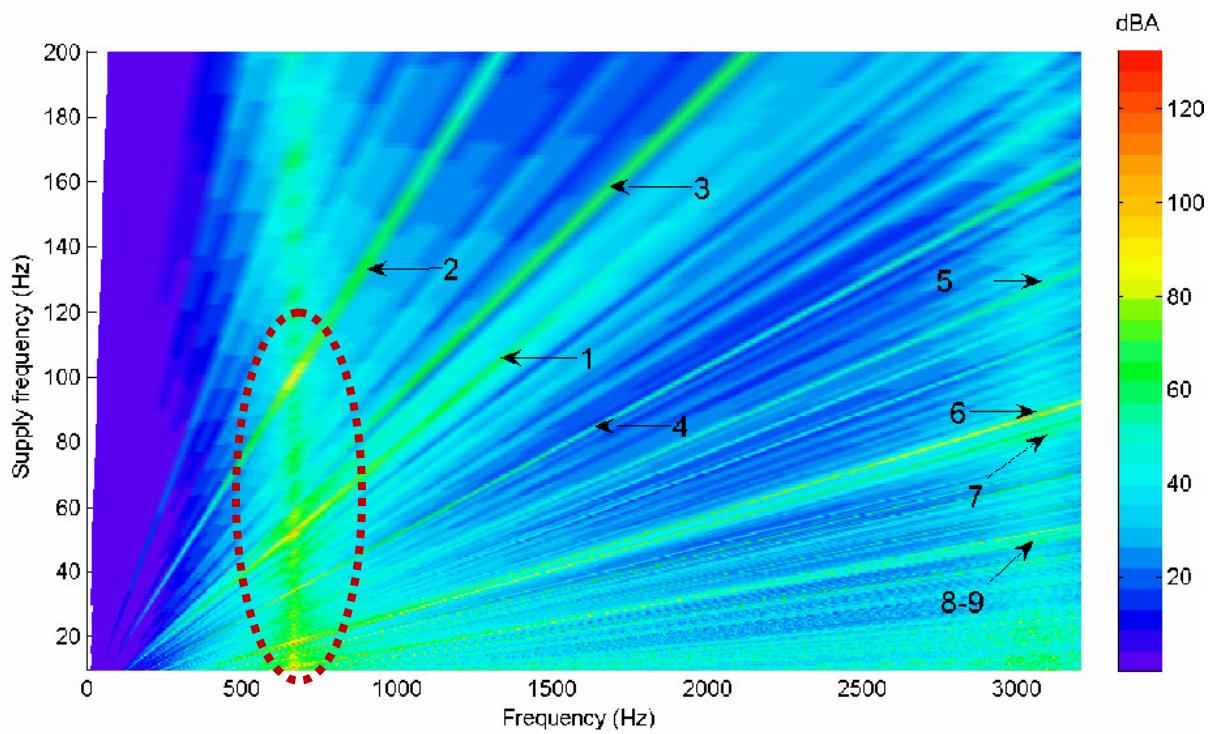


Figure 10: Simulated sonogram of a water-cooled 250 kW traction motor in sinusoidal off-load case ( $f_s=0$  to 200 Hz).

We can see that the simulation tool DIVA correctly predicts the main resonance, and all the main noise spectrum lines. One can prove that line 2 is due to a winding harmonic vibration, line 1 to a saturation harmonic vibration of order 2 which resonates with the stator elliptical mode near 700 Hz, and lines 3 to 9 are slotting lines. The differences in noise levels are mainly due to the fact that the experimental sonogram was measured with a 50 dBA ambient noise, whereas numerical simulation does not contain any ambient noise.

Figure 11 shows an acceleration spectrogram of a PWM fed motor. Slotting lines, PWM lines and slotting PWM lines appear at predicted frequencies.

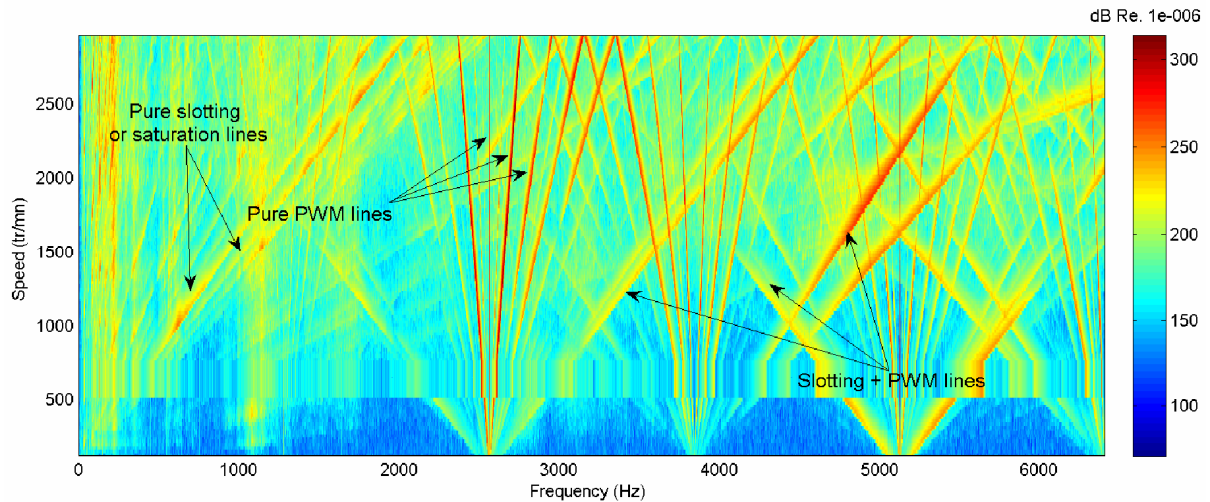


Figure 11: Experimental spectrogram of a traction motor in PWM case.

## 5 APPLICATION

As the simulation tool and the analytical expressions of Maxwell force lines have been extensively validated [14-18] with tests and/or FEM, they can be used to design new ALSTOM motors. This is done acting on both the motor geometry, mainly through the slot number combination, and the motor PWM strategy. The model has been also coupled to a multi-objective optimization tool in order to find the quietest motors fulfilling the required traction performances (efficiency, torque, etc) [12,13,19].

### 5.1 Slot numbers combination

We have seen that the slot numbers combination  $Z_r$  and  $Z_s$  have a great influence on magnetic noise due to slotting vibrations, as they determine the spatial orders of the vibrations. Some experimental [23] or empirical rules exist, but they cannot pretend to be general as they depend on the motor natural frequencies, and on the starting phase speed range. To avoid large magnetic forces (low  $k_r$  and  $k_s$ ) with low spatial modes, some exhaustive noise simulations have been run on a typical ALSTOM traction motor which is run from 0 to 3500 rpm. The average noise and maximum noise have thus been computed for  $Z_r$  going from 20 to 100, and  $Z_s$  from 12 to 96 for  $p=2$ , and 18 to 108 for  $p=3$ .

This database is now used by ALSTOM engineers to properly choose the rotor and stator slot numbers, avoiding the excitation of low order modes by magnetic forces.

### 5.2 PWM strategy

Noise due to PWM vibrations is limited by avoiding the match between the exciting frequencies around twice the switching frequency and  $0$  or  $2p$  stator modes natural frequencies.

Moreover, as seen in Table 2, the PWM noise is mainly determined by three lines of frequencies  $2f_c$ ,  $2f_c+f_s$  and  $2f_c-f_s$ : when  $f_s$  is close to 0, these three lines are very close one to another, creating an unpleasant sound characterized by a high roughness [28]. Some new PWM strategies with low psycho-acoustic impact are therefore investigated.

### 5.3 Optimizations

DIVA has been coupled to the evolutionary optimization algorithm NSGA-II [29]. This way, an optimization has been run in order to design a new quiet motor which fulfills the specified torque/speed curve, and does not degrade the aimed efficiency. The optimization results, combined to the slot combination rules, helped defining two low-noise prototypes which should respectively improve the maximum magnetic noise levels of 6 dBA and 14 dBA, and the average noise of 7 dBA and 10 dBA.

## 6 CONCLUSIONS

A fully analytical model of the audible magnetic noise radiation of a PWM-fed induction machine has been built to help ALSTOM designing low magnetic noise motors. This model was implemented in fast simulation tool, DIVA, which was validated at different stages, using electromagnetic and mechanical FEM software, and advanced vibro-acoustic tools such as operational deflection shapes, experimental and operational modal analysis, sonograms and spectrograms.

The analytical expressions of the largest magnetic forces magnitude, frequency and spatial order have been derived, which allowed a deeper understanding of the magnetic noise phenomenon and the establishment of low-noise design rules.

This fast and efficient simulation tool helps designing new motors and new PWM strategies improving the noise level on the whole speed range. It also allows quickly diagnosing and solving the magnetic noise issues occurring on current projects. DIVA has been coupled to an optimization tool, which helped designing two new ALSTOM motor prototypes with low noise and high efficiency. At resonance, the expected magnetic noise improvements are respectively 14 dB, and 10 dB.

## 7 ACKNOWLEDGEMENTS

The authors acknowledge the support of the ADEME for this work (Predit III – PROSODIE project).

## 8 REFERENCES

- [1] A. Ait-Hammouda, *Prédimensionnement et étude de sensibilité vibro-acoustique de machines à courant alternatif et à vitesse variable*, Ph.D. dissertation (USTL, Lille, France, 2005).
- [2] P. Alger, *The Nature of Polyphase Induction Machines* (John Wiley & Sons, Inc., 1951).
- [3] G. Bossio, C. De Angelo, J. Solsona, G. Garcia and M.I. Valla, “A 2-D model of the induction machine: an extension of the modified winding function approach,” *IEEE Trans. on Energy Conversion*, **19**(1), 2004.
- [4] J. F. Brudny, “Modélisation de la denture des machines asynchrones : phénomènes de résonances,” *J. Phys. III*, **37**(7), 1997.
- [5] A. Fasquelle, A. Ansel, S. Brisset, P. Borchet and A. Randria, “Iron losses distribution in a railway traction induction motor,” *Proceedings of ICEM* (2006).
- [6] A. Ghoggal, M. Sahraoui, A. Aboubou, S.E. Zouzou and H. Razik, “An improved model of the induction machine dedicated to faults detection – extension of the

- modified winding function approach,” *Proceedings of IEEE Int. Conf. on Industrial Technology* (2005), pp. 191–196.
- [7] J.F. Gieras, C. Wang and J.C. Lai, *Noise of polyphase electric motors* (CRC Press, 2005).
- [8] I. Hirotsuka, K. Tsuboi and F. Ishibashi, “Effet of slot-combination on electromagnetic vibration of squirrel-cage induction motor under loaded condition,” *Proceedings of Power Conversion Conference* (1997).
- [9] A. Hubert, *Contribution à l'étude des bruits acoustiques générés lors de l'association machines électriques - convertisseurs statiques de puissance. Application à la machine asynchrone*, Ph.D. dissertation (Université des Technologies de Compiègne, France, 2000).
- [10] H. Jordan, *Electric motor silencer - formation and elimination of the noises in the electric motors* (W. Giradet-Essen editor, 1950).
- [11] V. Lanfranchi, A. Hubert and G. Friedrich, “Comparison of a natural sampling and a random PWM control strategy for reducing acoustic annoyances,” *Proceedings of the European Power Electronics and drive conference* (2003).
- [12] J. Le Besnerais, V. Lanfranchi, M. Hecquet, and P. Brochet, “Multiobjective optimization of the induction machine with minimization of audible electromagnetic noise,” *European Physics Journal – Applied Physics*, **39**(2), 2007.
- [13] J. Le Besnerais, V. Lanfranchi, M. Hecquet, and P. Brochet, “Multi-objective optimization of induction machines including mixed variables and noise minimization,” *IEEE Trans. on Mag.*, **44**(6), 2008.
- [14] J. Le Besnerais, V. Lanfranchi, M. Hecquet, P. Brochet, and G. Friedrich, “Acoustic noise of electromagnetic origin in a fractional-slot induction machine,” *COMPEL*, **27**(5), 2008.
- [15] J. Le Besnerais, A. Fasquelle, M. Hecquet, V. Lanfranchi, P. Brochet, and A. Randria, “A fast noise-predictive multiphysical model of the PWM-controlled induction machine,” *Proceedings of the International Conference on Electrical Machines* (2006).
- [16] J. Le Besnerais, A. Fasquelle, M. Hecquet, J. Pellé, V. Lanfranchi, S. Harmand, P. Brochet, and A. Randria, “Multiphysics modeling: electro-vibro-acoustics and heat transfer of induction machines,” *Proceedings of the International Conference on Electrical Machines* (2008).
- [17] J. Le Besnerais, V. Lanfranchi, M. Hecquet, P. Brochet, and G. Friedrich, “Characterisation of the radial vibration force and vibration behaviour of a PWM-fed fractional-slot induction machine,” *IET Power Application*, accepted for publication.
- [18] J. Le Besnerais, V. Lanfranchi, M. Hecquet, and P. Brochet, “Bruit audible d'origine magnétique des machines asynchrones,” *Techniques de l'Ingénieur*, **D6**(D 3580), 2008.
- [19] J. Le Besnerais, A. Fasquelle, V. Lanfranchi, M. Hecquet, and P. Brochet, “Mixed-variable optimal design of induction motors including efficiency, noise and thermal criteria,” *Proceedings of the International Conference on Engineering and Optimization* (2008).
- [20] M. Liwschitz, *Calcul des machines électriques* (Spes Lausanne, 1967).
- [21] W. C. Lo, C. C. Chan, Z. Q. Zhu, L. Xu, D. Howe and K. T. Chau, “Acoustic noise radiated by PWM-controlled induction machine drives,” *IEEE Trans. on Ind. Elec.*, **47**(4), 2000.
- [22] K.C. Maliti, *Modelling and analysis of magnetic noise in squirrel-cage induction motors*, Ph.D. dissertation (Royal Institute of Technology, Dpt. of Electric Power Engineering, Stockholm, Sweden, 2000).
- [23] Y. Okuyama and S. Moriyasu, “Electromagnetic noise of induction motors driven by PWM inverters,” *Electrical Engineering in Japan*, **133**(3), 2000.

- [24] P.L. Timar, *Noise and vibration of electrical machines* (Elsevier, 1989).
- [25] P.L. Timar, "Acoustic noise of electromagnetic origin in an ideal frequency-converter-driven induction motor," *IEE Proc. on Elec. Power Appl.*, **141**(6), 1994.
- [26] S.P. Verma and A. Balan, "Experimental investigations on the stators of electrical machines in relation to vibration and noise problems," *IEE Proc. on Elec. Power Appl.*, **145**(5), 1998.
- [27] S.J. Yang, *Low noise electrical motors* (Clarendon Press, Oxford, 1981).
- [28] E. Zwicker and H. Fastl, *Psychoacoustics, Facts and Models* (Springer-Verlag, Berlin Heidelberg, Germany, 1992).
- [29] K. Deb, A. Pratap, S. Agarwal and T. Meyarivan, "A fast and elitist multiobjective genetic algorithm: NSGA-II", *IEEE Trans. on Ev. Comp.*, **6**(2), 2002.